Diffuse Optical Tissue Simulator (DOTS): An Experimental Calibrating System for Functional DOT Imaging

R. L. Barbour[1,2], H. L. Graber[1,2], Y. Xu[1,2], Y. Pei[1], R. Ansari[1], M.B. Levin[1], M. Farber[2]

[1]NIRx Medical Technologies LLC, 15 Cherry Lane, Glen Head, NY 11545
[2]SUNY Downstate Medical Center, 450 Clarkson Ave., Brooklyn, NY 11203

I. Introduction

In this report we introduce the concept of employing electrochromic (EC) materials as a basis for developing programmable calibrating phantoms that are capable of accurately mimicking a broad array of optical responses observed in tissues using NIR technology.

EC materials comprise a large class, ranging from conducting polymers to liquid crystals. Notably, by simply applying a current source, these materials can be made to vary in their optical absorption, scattering, or fluorescent properties, over a wide range of operating conditions.

II. The Calibrating Phantom

Desired Properties
- Long shelf life
- Good repeatability
- Large dynamic range
- Freely programmable
- Adaptable to various tissue-like backgrounds
- Fast response time

Intended Uses
- Quality assurance indicator of instrument performance.
- Training device for improving operator skill in use of optical measuring heads.
- Benchmarking tool for algorithm performance.
- Validation of observed responses.

III. Approach to Constructing Phantom

1. Construct anatomical phantom using silicone rubber doped with TiO_2 as scattering medium and black carbon as dye.
   a. Generate cast of cortex containing embedded EC cells, measuring ~10×10×0.2 mm, at desired positions (prefrontal, frontal, MC, OC).
   b. Place cast inside plastic skull.
   c. Fill spaces using clear silicone rubber to mimic CSF.
2. After curing, apply measuring helmet containing optical leads.
3. Drive EC cell according to desired dynamic response.
4. Perform dual-wavelength measurement.
5. Reconstruct image time series.
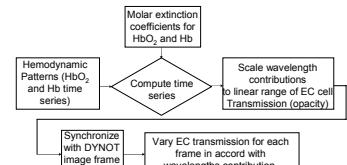
IV. Control of Phantom

Figure 1. Block diagram of the procedure for mimicking hemodynamic time series with EC cells.
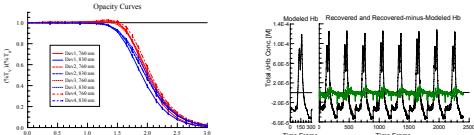

Figure 2. Opacity response curves of EC cells to applied voltage measured at 760 and 830 nm. Error bars identify SD over a 1 min period.
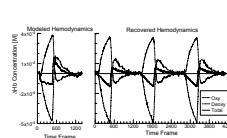

Figure 3. Modeled and observed test functions mimicking a blood volume change, and recovery error (i.e., difference between recovered and modeled).

Figure 4. Modeled response to cuff ischemia, and measured response to three consecutive trials using EC cell.

Figure 5. DOTS Phantom, LabVIEW control interface and EC cell positions.

V. Data Analysis

i. Image Reconstruction

Treat inverse problem as a linear perturbation equation, with the perturbation formulation relating the measured data to a selected reference medium using a system of linear equations with the form

$$\mathbf{u} - \mathbf{u}_r = \delta\mathbf{u} = \mathbf{W}_r \delta\mathbf{x} \quad (1)$$

- $\delta\mathbf{x}$ = position-dependent difference between optical properties (i.e. absorption coefficients) of target and reference media
- $\delta\mathbf{u}$ = vector of differences between measured light intensities ($\mathbf{u}$) and those predicted for a selected reference medium ($\mathbf{u}_r$)
- $\mathbf{W}_r$ = Jacobian operator

The "**Normalized Difference Method**" (NDM) approximation relates all source-detector pairs to the medium properties:

$$\delta\mathbf{x} = \mathbf{W}_r^{-1}(\mathbf{u}_1 - \mathbf{u}_r) + \mathbf{W}_r^{-1}(\mathbf{D}_{u_r}\mathbf{D}_{u_2}^{-1} - \mathbf{I})\mathbf{u}_1 \quad (2)$$

- $\mathbf{I}$ = identity matrix
- $\mathbf{D}_{ur}$ and $\mathbf{D}_{u2}$ = diagonal matrices for vectors $\mathbf{u}_r$ and $\mathbf{u}_2$, respectively

1. The first term in Eq2 is the solution that would be obtained by solving the standard perturbation problem (Eq1)
2. The second term in Eq2 is a correction factor whose value is a function of the accuracy of the selected reference medium
3. $\mathbf{W}_r$ and $\mathbf{u}_r$ are obtained from a reference medium, and are therefore matched to each other
4. The NMD is more robust, and is less sensitive to noise and instrumentation variables related to the acquisition of data (i.e. fiber contact with skin, subject motion, etc.).
5. This formulation is solved using standard numerical algebraic techniques, including
   - Truncated Single Value Decomposition or
   - Regularized LU Decomposition

ii. Image Enhancement by Linear Deconvolution

Linear Spatial Deconvolution reduces image blurring that occurs with first-order solutions:
- Absorption coefficient μ_a in a test medium is "tagged" in every pixel with a unique time-varying function.
- Thus, it is possible to construct a filter matrix $\mathbf{F}$ that solves the equation $\mathbf{v} = \mathbf{Fu}$, where $\mathbf{u}$ is the reconstructed image and $\mathbf{v}$ is the test medium.
- The matrix $\mathbf{F}$ can subsequently be applied to experimental data, such that the image result is more accurate.
In practice, the matrix of experimental absorption coefficients $\mathbf{X}$ is difficult to invert, and the equation $\mathbf{Y} = \mathbf{FX}$ is unsolvable. A commonly used strategy is to try to minimize the difference matrix $\mathbf{Y} - \mathbf{FX}$ by selecting elements of $\mathbf{F}$, f_{ji}, such that the sum of the squares of the errors in the individual terms when $\mathbf{Y}$ is approximated by $\mathbf{FX}$ is minimized (Eq3)

$$I = \min \sum_{k=1}^{N_t} \sum_{j=1}^{N_s} \left(y_{jk} - \sum_{i=1}^{N_s} f_{ji} x_{ik} \right)^2 \quad (3)$$

Setting the derivative of I with respect to each element of $\mathbf{F}$ equal to zero yields Eq4

$$\sum_{k=1}^{N_t} y_{jk} x_{ik} = \sum_{k=1}^{N_t} \sum_{l=1}^{N_s} f_{jl} x_{lk} x_{ik} \quad (4)$$

This is the matrix equation $\mathbf{YX}^T = \mathbf{FXX}^T$, where $\mathbf{X}^T$ is the transpose of $\mathbf{X}$, and $\mathbf{XX}^T$ can be inverted to yield $\mathbf{F} = (\mathbf{YX}^T)(\mathbf{XX}^T)^{-1}$.

iii. Feature Extraction

"**General Linear Model**" (GLM) is able to extract the extent to which certain measurable parameter fluctuations (e.g., vital-sign measurements during experiments) are present in the time series at each pixel in the image. These "model functions" are related to the recovered time series via Eq5

$$\boldsymbol{\mu} = \mathbf{A}\boldsymbol{\beta} + \boldsymbol{\varepsilon} \quad (5)$$

- $\boldsymbol{\mu}$ = matrix of absorption values
- $\mathbf{A}$ = matrix of model functions
- $\boldsymbol{\beta}$ = matrix of fitting parameters
- $\boldsymbol{\varepsilon}$ = matrix of residual errors.
Solution of the model involves finding the $\boldsymbol{\beta}$ that minimizes $\boldsymbol{\varepsilon}$.
At each position and for each coefficient, it is possible to calculate a t-statistic and associated p-value to test the hypothesis that the observed coefficient value could be obtained by chance.
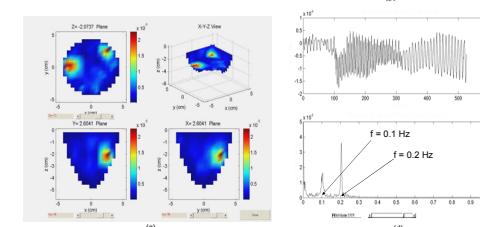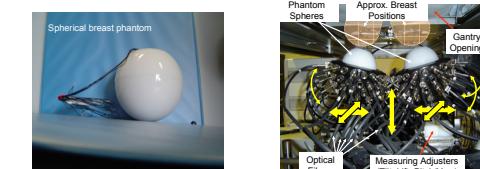
VI. Experimental Results with Breast Phantom

Figure 6. (a) DOTS Phantom for optical mammography, containing two independently controllable EC devices; (b) corresponding measuring head; (c) representative recovered image from the phantom-medium time series measurement; (d) μ_a time series, and its amplitude spectrum, recovered from a pixel within one of the EC devices.

- Fig. 6(a) Laboratory phantom medium
  - Approximates size and shape of a breast
  - Has defined background optical coefficient values
  - Contains a pair of electrochromic devices
    - Independently controllable
    - Absorption coefficient (μ_a) can be changed by adjusting the applied voltage
    - Can be programmed to produce a pre-selected μ_a time series.
- Fig. 6(b) DYNOT simultaneous dual-breast measuring head
  - Data collected from 124 channels (62 fibers × 2 wavelengths) in parallel
  - Sources location is time-multiplexed
  - Measurement rate: 2 complete image frames (> 3×10⁴ data points) per second
- Experimental test shows that DYNOT imager:
  - Fig. 6(c) Accurately localizes an idealized lesion inside the medium
  - Fig. 6(d) Detects the programmed signals with high temporal fidelity
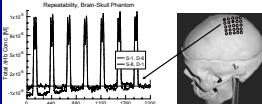
VII. Experimental Result with Brain Phantom

Figure 7. Measured Hb total changes mimicked using LC cell embedded in head phantom, minus skull. Phantom contains cerebral cortex molded from anatomical model, and an overlying clear CSF space. Depth of LC cell ~1 cm below surface. Background μ_a = 0.04 cm⁻¹; μ_s = 7 cm⁻¹. Red dots indicate position of illustrated measuring sites from reciprocal channels.
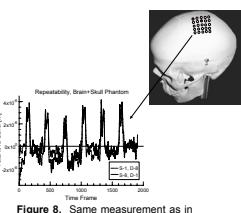

Figure 8. Same measurement as in Figure 4, except with skull in place.
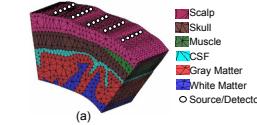

Figure 9. (a) Segmented MR brain map containing indicated tissue types; (b) volume rendered image shown location of dynamic inclusion embedded in gray matter; (c) modeled dynamic response of the EC cell.
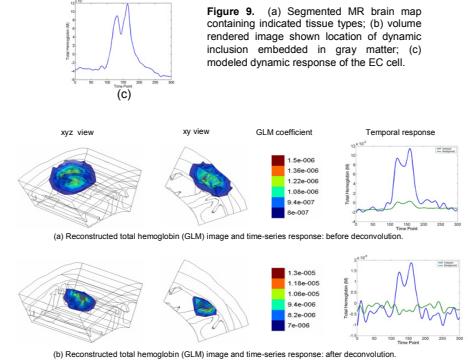

Figure 10. Brain Phantom with Skull: 3D Reconstructed total hemoglobin (GLM) image.
(a) Reconstructed total hemoglobin (GLM) image and time-series response: before deconvolution.
(b) Reconstructed total hemoglobin (GLM) image and time-series response: after deconvolution.

Figures 7 and 8 show the response obtained, using the temporal opacity adjustment scheme applied to an EC cell embedded in a head-shaped phantom composed of absorbing and scattering materials that closely match the known optical properties of human skull and brain tissue. For illustrative purposes, we have identified the responses seen by a reciprocal pair of illumination-detection fibers within a larger 5×5 array of illuminating fibers. Inspection of the curves plotted in Fig. 7 reveals that, even when the EC cell is embedded in a surrounding scattering medium, we can still accurately mimic the Valsalva response with high repeatability. In Figure 8 we show a similar response, except here we have introduced the overlying skull in order to more accurately mimic an actual response from a human subject. Repeatability of the considered response is evident, albeit with a higher noise level.

Figure 10 shows the results obtained when the acquired time-series optical array data illustrated in Figure 9 is subjected to image reconstruction using the Normalized Difference Method and additionally processed to produce a volumetric image of the considered temporal behavior via a GLM computation. For the considered case, the finite element mesh employed was derived from an MR prior of the motor cortex area, which is the same area explored in the head phantom and for convenience is illustrated in a surface [Fig. 9(a)] and volume rendering [Fig. 9(b)]. Comparison of Fig. 9(c) and the recovered time courses in Fig. 10 shows that the considered hemodynamic response can be accurately recovered.